Statistical Characterization of GLONASS Broadcast Clock Errors and Signal-In-Space Errors

Liang Heng, Grace Xingxin Gao, Todd Walter, and Per Enge,
Stanford University

BIOGRAPHY

Liang Heng is a Ph.D. candidate under the guidance of Professor Per Enge in the Department of Electrical Engineering at Stanford University. He received his B.S. and M.S. degrees in electrical engineering from Tsinghua University, Beijing, China. His current research interests include GNSS integrity and modernization.

Grace Xingxin Gao, Ph.D., is a research associate in the GPS lab of Stanford University. She received the B.S. degree in mechanical engineering and the M.S. degree in electrical engineering, both at Tsinghua University, Beijing, China. She obtained the Ph.D. degree in electrical engineering at Stanford University. Her current research interests include GNSS signal and code structures, GNSS receiver architectures, and interference mitigation. She has received the Institute of Navigation (ION) Early Achievement Award.

Todd Walter, Ph.D., is a senior research engineer in the Department of Aeronautics and Astronautics at Stanford University. He received his Ph.D. from Stanford and has worked on extensively on the Wide Area Augmentation System (WAAS). He is currently working on dual-frequency, multi-constellation solutions to provide aircraft guidance. He has received the Thurlow and Kepler awards from the ION. He is a fellow of the ION and currently serves as its president.

Per Enge, Ph.D., is a Professor of Aeronautics and Astronautics at Stanford University, where he is the Kleiner-Perkins, Mayfield, Sequoia Capital Professor in the School of Engineering. He directs the GPS Research Laboratory, which develops satellite navigation systems based on the Global Positioning System (GPS). He has been involved in the development of WAAS and LAAS for the FAA. Per has received the Kepler, Thurlow and Burka Awards from the ION for his work. He is also a Fellow of the ION and the Institute of Electrical and Electronics Engineers (IEEE). He received his PhD from the University of Illinois in 1983.

ABSTRACT

With more than 70 navigation satellites orbiting the Earth, global navigation satellite systems (GNSS) users are fascinated to use multiple constellations to enhance positioning availability, accuracy, integrity, continuity, and robustness. As the Russian Global'naya Navigatsionnaya Sputnikovaya Sistema (GLONASS) has fully restored its constellation, not only does a combination of GLONASS and the Global Positioning System (GPS) attract ever-increasing multi-constellation-based navigation applications, but it also serves as a ready-made proving ground for various next-generation multi-constellation GNSS integrity monitoring systems. Although both GLONASS and GPS employ the same concept of time-of-arrival positioning, GLONASS is different from GPS in terms of constellation design, signal modulation, ephemeris format, atomic frequency standards, ground monitor facilities, etc. These differences may make GLONASS show a different signal-in-space (SIS) behavior from GPS. A thorough characterization of GLONASS SIS errors helps the development of multi-constellation GNSS integrity monitoring systems such as advanced receiver autonomous integrity monitoring.

Broadcast ephemeris and clock errors are two dominant factors in SIS user range errors (UREs). As an extension of our previous paper on broadcast GLONASS ephemeris errors, this paper introduces broadcast GLONASS clock errors and focuses on resultant SIS UREs. Broadcast GLONASS clocks are propagated from validated GLONASS navigation messages, which are generated from all the GLONASS navigation data logged by the International GNSS Service (IGS) volunteer stations. Raw GLONASS clock errors are derived from a comparison between broadcast clocks with the precise clock solutions from three IGS Anal-

ysis Centers. Although the three solutions do not agree with each other due to unknown time-variant common biases, we overcome this difficulty via a clock alignment algorithm. The ephemeris errors computed in our previous paper and the aligned clock errors are combined into four metrics of SIS user range errors (UREs). An outlier filter and a few robust statistics techniques are used to cope with anomalous satellite behaviors and data-logging errors.

We first analyze long-term stationarity of SIS URE performance to determine the time span for the statistics. The clock errors and SIS UREs in the last three years are then characterized with respect to mean and standard deviation, distribution, correlation among satellites, and geographic dependency. The results show that 1) clock error behavior dominate SIS URE behavior; 2) clock errors and SIS UREs are usually biased and super Gaussian distributed; 3) SIS UREs of different satellites are usually slightly correlated, but the heavy tail of chi-square statistics may imply large UREs occasionally occurring on several satellites simultaneously. These results indicate that the traditional independent, zero-mean Gaussian assumptions for SIS UREs are too ideal. In addition, due to limited geographic distribution of GLONASS ground monitor stations, we observe that SIS URE performance of a satellite is partially dependent on whether the satellite is monitored.

INTRODUCTION

Besides the United States' Global Positioning System (GPS), the Russia's Global'naya Navigatsionnaya Sputnikovaya Sistema (GLONASS) is so far the only fully developed global navigation satellite system (GNSS). At the time of writing, the GLONASS constellation is full of 24 operational satellites [1] and capable of practical global continuous navigation [2]. The utilization of both GLONASS and GPS constellations enhances positioning availability, accuracy, integrity, continuity, and robustness with better satellite geometries and more redundant observation data, especially for the mitigation of radio frequency interferences [3], the navigation in high latitudes [4, 5], and the use of receiver autonomous integrity monitoring (RAIM) [6, 7].

GLONASS employs the same concept as GPS, time-of-arrival positioning, in which the measured distance from a user receiver to at least four satellites in view as well as the positions and clocks of these satellites are the prerequisites for the user receiver to fix its exact position [8]. For most users, real-time satellite positions and clocks are derived from ephemeris parameters and clock correction terms in broadcast navigation messages generated by the control segment on the basis of a prediction model and the measurements at several monitor stations [9, 10]. The differences between the broadcast ephemerides/clocks and the truth account for signal-in-space (SIS) errors, which are mainly contributed by the errors due to the

- Space Segment, such as satellite acceleration uncertainty, clock instability, satellite antenna variation [11], and signal imperfection, and the errors due to the
- Control Segment, such as estimation errors, prediction errors, and curve fit errors in broadcast ephemerides and clocks.

As one of the major error sources of pseudorange measurement inaccuracy, SIS errors directly affect the positioning accuracy and integrity. A thorough understanding of SIS errors is important not only for assessing the general system performance but also for developing the next generation multi-constellation GNSS integrity monitoring system.

Usually, SIS performance are evaluated with respect to accuracy and integrity. The SIS accuracy is mainly related to nominal core SIS errors, whereas the integrity is mainly related to anomalous tail SIS errors. For GPS, the nominal SIS errors have been extensively studied in [12–17], and the anomalous SIS errors have been studied in [15, 16, 18–22]. For GLONASS, although there have been some relevant prior work [23–25], thorough studies on nominal and anomalous SIS errors are of great need. Following our previous paper on broadcast GLONASS ephemeris errors [26], this paper includes broadcast GLONASS clock errors, and focuses on a thorough statistical characterization of nominal GLONASS SIS errors.

In this paper, we employ a methodology similar to [17, 26]. Clock errors are computed by comparing broadcast clocks with several versions of precise clocks. SIS user range errors (UREs) are computed from the ephemeris errors in [26] and the aligned clock errors. Both clock errors and SIS UREs are then characterized with respect to long-term stationarity, mean and standard deviation, distribution, correlation among satellites, and geographic dependency. For the rest of this paper, we start with a description of the data sources. Then, we elaborate on the methodology. Finally, we present the statistics of the GLONASS clock errors and SIS errors over the past three years.

DATA SOURCES

Broadcast GLONASS clocks

Broadcast GLONASS navigation message data are publicly available at International GNSS Service (IGS) [27], archived in the Receiver Independent Exchange Format (RINEX) [28]. These data include the immediate information in the GLONASS broadcast navigation message [29] such as reference time, clock correction, satellite position, satellite velocity, lunisolar acceleration, and healthy flag.

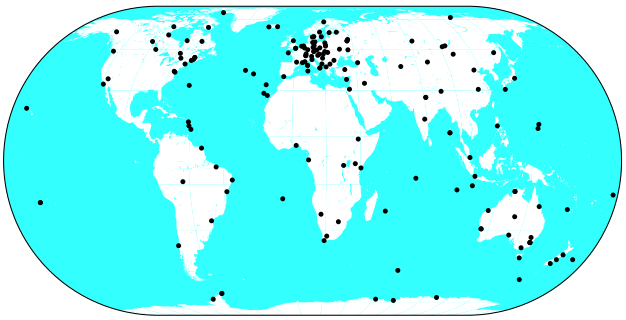

Figure 1. IGS GPS/GLONASS stations as of Jan 29, 2012 (adapted from `http://igscb.jpl.nasa.gov`)

Unfortunately, the RINEX format for GLONASS, unlike that for the GPS, does not include URA, probably because the old GLONASS satellites did not broadcast URA [29] when the RINEX format was defined.

As shown in Figure 1, the IGS tracking network comprises more than 100 GPS/GLONASS stations all over the world to ensure seamless, redundant data logging. Since broadcast navigation messages are usually updated every 30 minutes, no single station can collect all of these navigation messages. To save users' effort, an IGS archive site, Crustal Dynamics Data Information System (CDDIS), routinely generates daily global combined broadcast navigation message data files `brdc`*`ddd`*`0.yyg` (or `igex`*`ddd`*`0.yyg` before December 2004) [30]. Unfortunately, these files sometimes contain errors due to accidental bad receiver data and various hardware/software bugs, as described in [26]. Therefore, we have devised and implemented a data cleansing algorithm to generate our own daily global combined GLONASS navigation messages, `sugl`*`ddd`*`0.yyg`[1], from all available raw navigation message data collected by all the IGS GPS/GLONASS stations. In order to make `sugl`*`ddd`*`0.yyg` as close as possible to the navigation messages that the GLONASS satellites actually broadcast, the data cleansing algorithm decides every value in a navigation message using majority voting. Therefore, all values in `sugl`*`ddd`*`0.yyg` are cross-validated. Accordingly, we refer to the `sugl`*`ddd`*`0.yyg` files as "validated navigation messages." The details of the data cleansing algorithm will be discussed in [31].

Precise GLONASS clocks

Although IGS has provided GLONASS precise ephemerides `igl`*`wwwwd`*`.sp3` (or `igx`*`wwwwd`*`.sp3` before December 2004) since at least 1999, there are still no precise GLONASS clocks available [32]. In fact, `igl`*`wwwwd`*`.sp3` is a weighted-mean combination of the independent solutions produced by a number of IGS Analysis Centers (ACs). Each AC routinely post-processes the observation data collected by some IGS GPS/GLONASS stations using its own processing strategy. The list below shows the IGS ACs' products that contain at least precise GLONASS ephemerides.

bkg[2] GPS + GLONASS, w/o precise clocks, data available till May 21, 2011

cod[3] GPS + GLONASS, w/o precise clocks

emx[4] GPS + GLONASS, w/ precise clocks, data available since Sep 11, 2011

esa[5] GPS + GLONASS, w/ precise clocks, data available since Oct 18, 2008

gfz[6] GPS + GLONASS, w/ precise clocks, data available since Apr 11, 2010

grg[7] GPS + GLONASS, w/o precise clocks, data available since Jan 9, 2011

iac[8] GLONASS only, w/ precise clocks

mcc[9] GLONASS only, w/o precise clocks, for only a few satellites

Among the eight products above, only four have precise GLONASS clocks. We have computed clock errors using these four versions of precise clocks, and Figure 2 shows the clock errors of GLONASS-M 721 (PRN[10] 13) over the last year. Apparently, the four versions of precise clocks do not exactly agree with each other. This may be one of the reasons why the `igl`*`wwwwd`*`.sp3` files do not to include precise GLONASS clocks.

However, as shown in Figure 3, a zoomed-in portion of Figure 2 reveals that these precise clocks could agree with each other if time-variant biases were removed.

Figure 4 further shows that, at any instant, the satellite clock errors computed from esa or gfz precise clocks are all offset by a common bias, while the clock errors computed from iac precise clocks do not show obvious biases[11]. This feature will help building a clock alignment algorithm to remove the

[1] The filename follows the convention of RINEX format. The prefix `sugl` stands for Stanford University GPS Laboratory.

[2] Produced by Bundesamt fuer Kartographie und Geodaesie, Germany

[3] Produced by Center for Orbit Determination in Europe, AIUB, Switzerland

[4] Producer unknown

[5] Produced by European Space Operations Center, ESA, Germany

[6] Produced by GeoForschungsZentrum, Germany

[7] Produced by CNES/CLS/GRGS, France

[8] Produced by Information-Analytical Center, Russia

[9] Produced by Mission Control Center, Russia

[10] As GLONASS uses FDMA rather than CDMA, "PRN" in this paper refers to orbit slot number.

[11] The comments in `iac`*`wwwwd`*`.sp3` files claim "S/V clocks are aligned to GPS & GLONASS time respectively using the broadcast ephemeris."

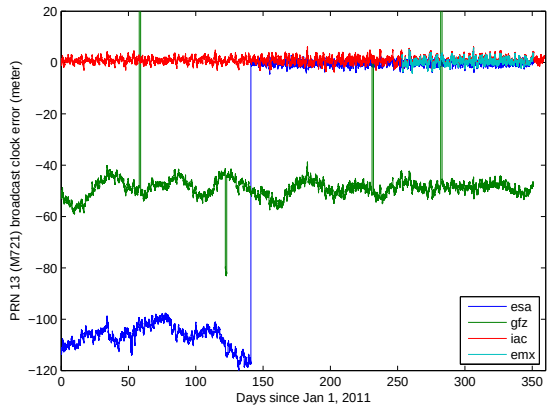

Figure 2. GLONASS-M 721 (PRN 13) clock errors in 2011, computed from esa, gfz, iac, and emx precise clocks. These precise clocks do not agree with each other.

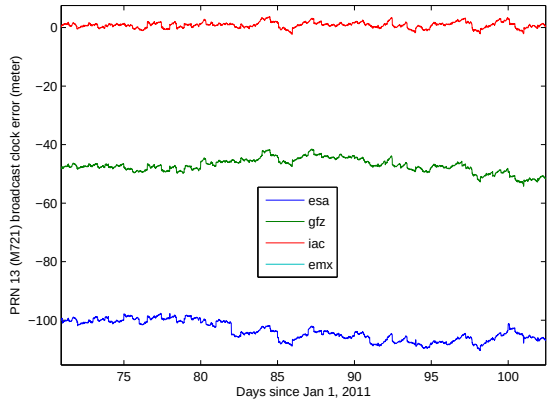

Figure 3. GLONASS-M 721 (PRN 13) clock errors from Day 71 to 103 of 2011, computed from esa, gfz, and iac precise clocks. These precise clocks could agree with each other if time-variant biases were removed.

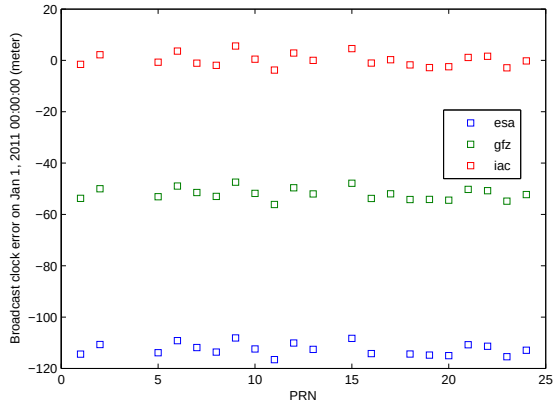

Figure 4. Clock errors of all satellites at 00:00:00 on Jan 1, 2011, computed from esa, gfz, and iac precise clocks. Common clock bias exists in esa and gfz precise clocks.

time-variant common biases. The clock alignment algorithm will be discussed in details in the section "Methodology."

METHODOLOGY

Figure 5 shows the framework of the whole process. According to the discussion in the section "Data Sources," we firstly use the data cleansing algorithm in [31] to vote validated items from the raw broadcast ephemeris/clock data, and then propagate them at 15-minute intervals synchronized to the precise ephemerides/clocks [26]. The precise ephemerides extracted from the `igl`*`wwwwd`*`.sp3` files are converted from satellite center of mass (CoM) to antenna phase center (APC); the difference between the propagated broadcast ephemerides and the precise ephemerides in APC are the raw ephemeris errors in the Earth-Centered, Earth-Fixed (ECEF) coordinate. The precise clocks extracted from the `esa`*`wwwwd`*`.sp3`, `gfz`*`wwwwd`*`.sp3`, and `iac`*`wwwwd`*`.sp3` files are compared with the propagated broadcast clocks; the differences are three versions of raw clock errors. After converting the ephemeris errors in the reference frame with respect to the space vehicle and aligning the raw clock errors, four metrics of SIS UREs can be computed and then statistical characterized. The algorithms used in each step will be discussed in the following subsections.

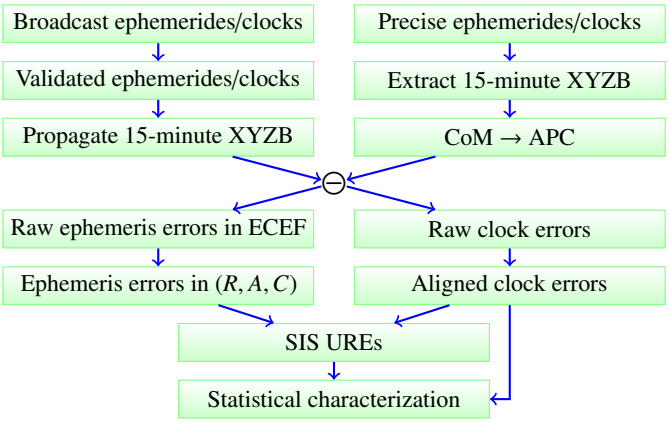

Figure 5. Framework of the whole process. XYZB values refer to the coordinates of satellite position and satellite clock bias.

Clock alignment

The analysis in the section "Data Sources" has implied that

- No obvious common clock biases exist in some precise clock products such as `iac`*`wwwwd`*`.sp3`;
- Common clock biases exist in some precise clock products such as `esa`*`wwwwd`*`.sp3` and `gfz`*`wwwwd`*`.sp3`;
- Common clock biases vary with time.

Accordingly, we model the common clock biases as follows:

$$\begin{aligned}
\mathrm{ClkErr}_{1,\mathrm{iac}} &= \mathrm{TrueClkErr}_1 + \epsilon_{1,\mathrm{iac}} \\
&\vdots \\
\mathrm{ClkErr}_{24,\mathrm{iac}} &= \mathrm{TrueClkErr}_{24} + \epsilon_{24,\mathrm{iac}} \\
\mathrm{ClkErr}_{1,\mathrm{esa}} &= \mathrm{TrueClkErr}_1 + \mathrm{CommonBias}_{\mathrm{esa}} + \epsilon_{1,\mathrm{esa}} \\
&\vdots \\
\mathrm{ClkErr}_{24,\mathrm{esa}} &= \mathrm{TrueClkErr}_{24} + \mathrm{CommonBias}_{\mathrm{esa}} + \epsilon_{24,\mathrm{esa}} \\
\mathrm{ClkErr}_{1,\mathrm{gfz}} &= \mathrm{TrueClkErr}_1 + \mathrm{CommonBias}_{\mathrm{gfz}} + \epsilon_{1,\mathrm{gfz}} \\
&\vdots \\
\mathrm{ClkErr}_{24,\mathrm{gfz}} &= \mathrm{TrueClkErr}_{24} + \mathrm{CommonBias}_{\mathrm{gfz}} + \epsilon_{24,\mathrm{gfz}}
\end{aligned}$$

In the above equations, $\mathrm{ClkErr}_{i,\mathrm{xxx}}$ is the clock error of PRN i computed from precise clocks `xxxwwwwd.sp3`, $\mathrm{TrueClkErr}_i$ is the true clock error of PRN i, $\mathrm{CommonBias}_{\mathrm{xxx}}$ is the common clock bias of the precise clocks `xxxwwwwd.sp3`, and $\epsilon_{i,\mathrm{xxx}}$ is the fitting error in $\mathrm{ClkErr}_{i,\mathrm{xxx}}$. The known values in the equations are marked in green, whereas the unknown variables we are interested in are marked in red.

Obviously, this is a typical system of linear equations in the $n+m-1$ unknown variables $\mathrm{TrueClockError}_i$, $\mathrm{CommonBias}_{\mathrm{esa}}$, and $\mathrm{CommonBias}_{\mathrm{gfz}}$, where n is the number of healthy satellites at the instant, and m is number of available precise clock products. Fortunately, this linear system is usually overdetermined because the number of equations, mn, exceeds the number of unknown variables, $n + m - 1$.

Since outliers may exist in $\mathrm{ClkErr}_{i,\mathrm{xxx}}$ due to either SIS anomalies or accidental errors in precise clocks, we use a robust multilinear regression to solve the overdetermined linear system. This robust multilinear regression uses iteratively reweighted least squares [33] with a bisquare weighting function [34]. Figure 6 (a) and (b) shows the solutions of the common clock biases and the sigma estimate of the fitting errors $\epsilon_{i,\mathrm{xxx}}$ during the past three years, respectively. One interesting phenomenon is that the esa precise clocks changed its time reference twice, and the latter change resulted in almost zero common clock biases but larger fitting errors. Another interesting phenomenon is that gfz precise clocks had a few spikes in the common clock biases, which may imply some anomalies of their time reference.

SIS error metrics

The raw broadcast and precise GLONASS ephemerides are in ECEF coordinate, so are the ephemeris errors. Greater insight can be provided if the ephemeris errors are represented in the reference frame with respect to the space vehicle: R—radial, A—alongtrack, and C—crosstrack. Besides, we

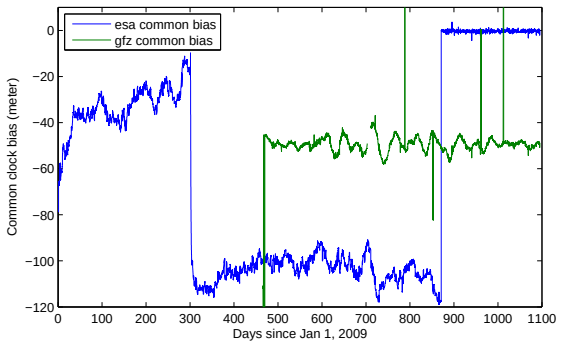

(a) Solutions of the common clock biases

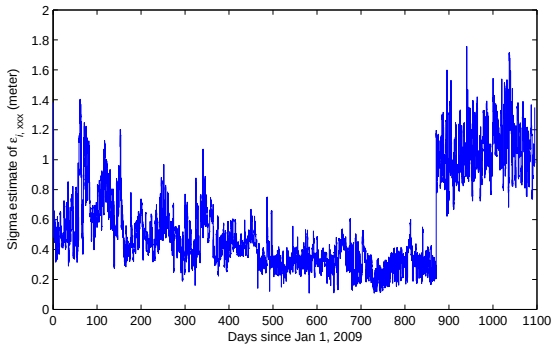

(b) Sigma estimate of fitting errors $\epsilon_{i,\mathrm{xxx}}$

Figure 6. Common clock biases and sigma estimates of fitting errors over the past three years.

use T to denote the aligned broadcast clock errors in meters.

For an arbitrary set of ephemeris and clock errors (R, A, C, T), GLONASS receivers at different locations on the Earth may experience different SIS UREs. Accordingly, the following four SIS error metrics are considered in this paper:

- Instantaneous SIS URE computed for 20 points spread evenly on the earth, as shown in Figure 7;
- Global average rms SIS URE given by [26]

$$\sqrt{(0.98R - T)^2 + (A^2 + C^2)/45}; \qquad (1)$$

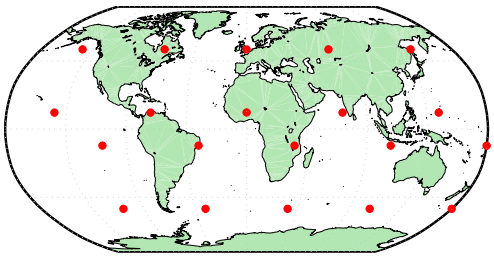

Figure 7. Instantaneous UREs are computed for 20 points spread evenly on the earth, which are derived from the vertices of a regular dodecahedron.

- Orbit-error-only rms SIS URE_O defined as

$$\sqrt{(0.98R)^2 + (A^2 + C^2)/45}; \tag{2}$$

- Worst-case SIS URE defined as

$$\max_{|\theta| \le 14.48^\circ} (R\cos\theta - T + \sqrt{A^2 + C^2}\sin\theta), \tag{3}$$

  where $\max(x)$ maximizes $|x|$ and return the corresponding x.

Worst-case URE can be computed either numerically from instantaneous UREs computed for a dense grid on the Earth or analytically from (R, A, C, T) [21, 35]. This paper uses the latter way.

Outlier filter

Since this paper focuses on the nominal core GLONASS SIS error behavior, the outliers due to residual data-logging errors in `sugl`*`ddd`*`0.yyg` files or true SIS anomalies are unwelcome to the statistics. In addition, the broadcast and the precise ephemerides and clocks have some build-in features to indicate "unhealthy" or "something happened". Therefore, the following outlier filters are used in this paper:

- Broadcast ephemerides and clocks: check health bits;
- Precise ephemerides and clocks: check event flags;
- Check if worst-case SIS URE greater than 50 meters,

where the fixed threshold of 50 meters is chosen for the following two reasons.

First, the statistics of nominal GLONASS SIS URE behavior in the section "Statistical Characterization" shows that the standard deviation of SIS UREs are generally less than 4 meters and the kurtosis of SIS UREs is around 2. Therefore, we can use 4 meters as the URA, and this value actually matches the broadcast URA most of the time. Moreover, a Student's t-distributed random variable X with parameter $\nu = 7$ has a kurtosis of 2, and $\text{Prob}(|X| > 11.2148) = 10^{-5}$. Accordingly, a 10^{-5} anomaly rate leads to a threshold of $4 \times 11.2148 \approx 45$ meters.

Second, the current GLONASS SIS UREs are roughly as twice large as the GPS SIS UREs before 2008. GPS defined a 30-meter threshold at that time [36]; similarly, a 60-meter threshold may apply to current GLONASS SIS UREs.

Considering both factors above, we finally choose a 50-meter threshold.

Robust statistics

Since SIS errors do not necessarily have a normal distribution, the traditional statistics such as mean, standard deviation, and correlation coefficient may be affected by some extreme samples. To cope with this problem, we use trimmed mean (also referred to as truncated mean) to measure the central tendency. A trimmed mean function $\text{mean}_\alpha(\cdot)$ is the mean after discarding the samples at the $50\alpha\%$ high end and $50\alpha\%$ low end. Analogously, a trimmed standard deviation function is defined as

$$\text{std}_\alpha(X) = \sqrt{\text{mean}_\alpha((X - \text{mean}_\alpha(X))^2)}. \tag{4}$$

In fact, a trimmed mean is a compromise between a mean and a median, and a trimmed standard deviation a compromise between a standard deviation and a median absolute deviation. In this paper, we use a small value $\alpha = 0.05$, i.e., use 95% of the data, to make the bias of both estimators small.

Normality metric

SIS errors are usually described or overbounded by a normal distribution. Hence, it is important to know how close the real errors are to normally distributed. Popular statistical hypothesis tests of normality, such as Jarque-Bera test, Shapiro-Wilk test, and Lilliefors test [37], usually reject the null hypothesis that the SIS errors comes from a distribution in the normal family. Even worse, common software implementations of these tests can seldom return a meaningful p-value [38] to tell how far SIS error samples are from normally distributed. Therefore, we use kurtosis to quantify normality. Kurtosis (also known as excess kurtosis) is defined as

$$\gamma(X) = \frac{\mathbb{E}(X - \mathbb{E}X)^4}{\left(\mathbb{E}(X - \mathbb{E}X)^2\right)^2} - 3. \tag{5}$$

A normal distribution has kurtosis $\gamma = 0$; a sub Gaussian distribution with light tails usually has kurtosis $\gamma < 0$; a super Gaussian distribution with heavy tails usually has kurtosis $\gamma > 0$.

Since kurtosis involves 4th-order statistics, it relies on extreme values but is vulnerable to statistical outliers. The "trimmed" method, discarding a certain percent of extreme samples, works well for estimating the mean and the standard deviation but introduces a significant bias for kurtosis. Alternatively, we compute kurtosis after discarding the samples with the absolute value greater than 6 times interquartile range. For a normal distribution, 6 times interquartile range is approximately equal to 8-sigma, equivalent to 1.2×10^{-15} tail probability. Because the sample size is less than 10^5 for each satellite, this tail probability ensures that only statistical outliers are discarded. This feature is important to a correct kurtosis estimation.

STATISTICAL CHARACTERIZATION

Long-term stationarity

Our previous study has shown that the GLONASS ephemeris error performance was stationary over the past three

years for almost the whole constellation [26]. With counting clock errors in, as shown in Figure 8, we found that the assumption of long-term stationarity is still true, except for GLONASS-M 729 and a few younger satellites. Therefore, this paper considers all available data during the past three years and the satellites active for at least one year in order to provide sufficient samples for the statistics.

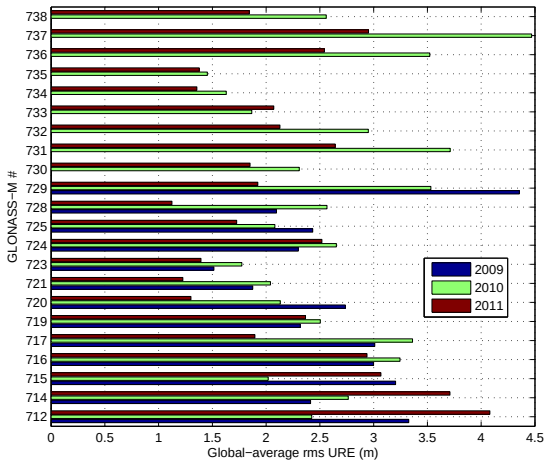

Figure 8. Global-average rms URE in 2009, 2010, and 2011.

Mean and standard deviation

Although SIS errors are generally assumed to follow a zero mean distribution, the reality may be different. Figure 9 plots the means of clock errors, instantaneous UREs, and worse-case UREs with a comparison to their standard deviations. It can be seen that most satellites have significant nonzero mean for their clock errors. For nearly a half of the satellites, the clock errors are so strongly biased that the mean of the clock errors is as large as the standard deviation. This performance, although does not quite match the GPS SIS performance [17], is much better than five years ago [23].

Besides, Figure 9 shows a close similarity among clock errors, instantaneous UREs, and worse-case UREs. This is a telling example to demonstrate that clock performance dominates SIS URE performance. In fact, this result is expected because clock errors are usually much larger than ephemeris errors [17, 26].

Distribution of SIS errors

In addition to mean and standard deviation, GLONASS clock errors and SIS UREs are further characterized in terms of distribution using the method described in the section

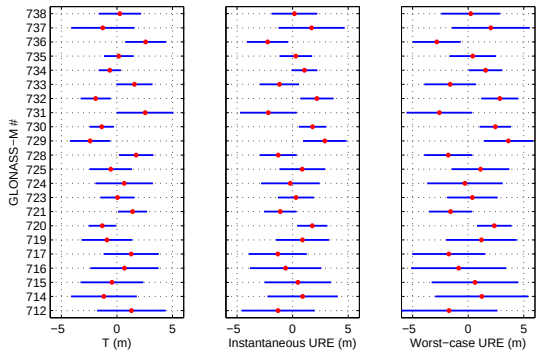

Figure 9. Mean of clock errors, instantaneous UREs, and worse-case UREs with a comparison to their standard deviations. The red dots indicate the mean, and the blue bars show the ± standard deviation.

"Methodology." Figure 10 shows the sample kurtosis of clock errors, instantaneous UREs, and worse-case UREs. Clearly, super Gaussian distribution is very common for clock errors and SIS UREs. About 4/5 satellites have $\gamma > 1$ and the average kurtosis of instantaneous UREs is approximately equal to 2.

For a more intuitive understanding of the distribution of SIS UREs, Figure 11 shows the Q-Q plots of the instantaneous UREs of two satellites: GLONASS-M 731 and GLONASS-M 732. The latter represents a typical super Gaussian distribution, whereas the former represents an atypical Gaussian distribution. We observed that not only the SIS UREs of most satellites have very heavy tails, but sometimes the distribution of the tails are also asymmetric. In practice, a normal distribution with inflated sigma may be used to overbound SIS UREs, or a more sophisticated distribution [39] should be considered.

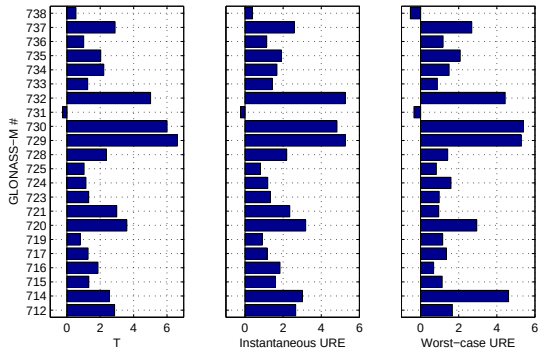

Figure 10. Sample kurtosis of clock errors, instantaneous UREs, and worse-case UREs. A positive value indicates a super Gaussian distribution with heavy tails.

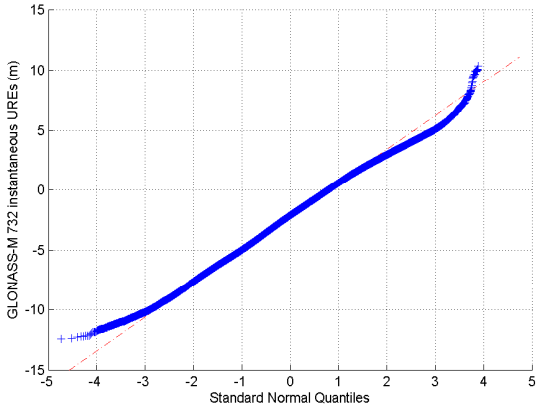

(a) GLONASS-M 731 instantaneous UREs
($\gamma = -0.23$, almost Gaussian, atypical)

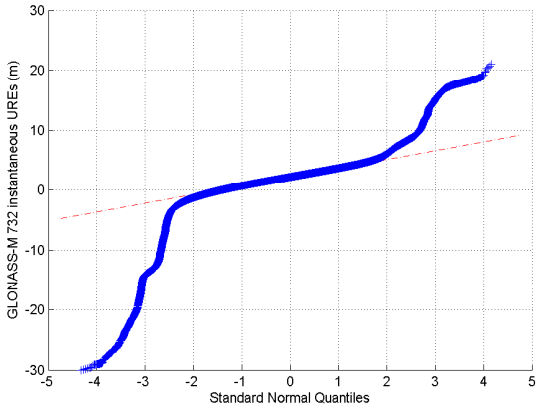

(b) GLONASS-M 732 instantaneous UREs
($\gamma = 5.26$, super Gaussian, typical)

Figure 11. Q-Q plots of the instantaneous UREs of GLONASS-M 731 and 732. Both satellites were launched at the same time, are in the same orbital plane, and have been being active for at least 600 days.

Correlation among satellites

In RAIM/ARAIM, one of the key assumptions is that large UREs occur on several satellites simultaneously with very low probability. In other words, for an arbitrary user on the Earth, the correlation among the UREs of the satellites in view is expected to be close to zero. With this assumption, if UREs are close to normal distributed, then the sum of their squares should be close to chi-square distributed. Therefore, multiple satellite monitoring in RAIM/ARAIM requires [15]

$$S = \sum_{i=1}^{k} \left(\frac{\mathrm{IURE}^i - \overline{\mathrm{IURE}}}{\mathrm{URA}^i} \right)^2 \le K^2_{\mathrm{prob}} = 50.2, \qquad (6)$$

where k is number of the satellites in view. Here we consider only one case $k = 8$, which happened the most frequently in last three years. Since the RINEX format for GLONASS does not include URA, we replace the URA in (6) by the sample standard deviations computed in the subsection "Mean and standard deviation."

Figure 12 plots S against the chi-square distribution with 7 degree of freedom (DoF) because the removal of the common clock error in (6) causes a loss of 1 DoF. The blue plus signs are the S computed from the real SIS UREs. It looks that the UREs of different satellites are highly correlated because the blue plus signs are high above the blue dash-dot line, which indicates the sum of squared Gaussian random variables. However, the real UREs are not normally distributed, and the analysis in the subsection "Distribution of SIS errors" has shown that they have an average kurtosis of 2. Accordingly, we plot the green dots using the sum of several squared Student's t-distributed random variables with parameter $\nu = 7$. A Student's t-distribution with $\nu = 7$ has a kurtosis of 2, which can be seen as an approximation of the distribution of SIS UREs. We tried the sum of 3 to 9 squared t-random variables, an the sum of 6 fits the majority of the blue plus signs best, as shown in Figure 12. Therefore, a possible quantification of the slight correlation among UREs of different satellites is that the correlation causes a loss of 1 degrees of freedom. Although the green dots can match the blue plus signs in terms of the core behavior, the tail of blue plus signs are much greater than the green dots. This is a strange phenomenon in comparison to GPS, for which we could make the tail of blue plus signs match the green dots [17]. One possible reason is that the SIS UREs are biased, as shown in the subsection "Mean and standard deviation," and these biases have caused large UREs occasionally occurring on several satellites simultaneously.

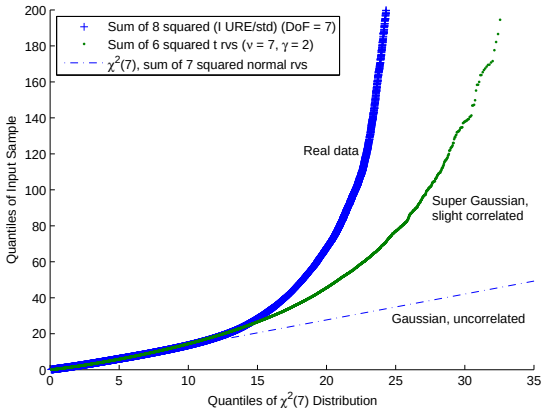

Figure 12. Chi-square values of real SIS UREs (blue plus signs) in comparison to uncorrelated Gaussian (blue dashed line) and slightly correlated super Gausian (green dots).

Geographic dependency

While GPS has distributed its monitor stations worldwide [10], GLONASS SIS still relies on a few monitor stations within the Russian territory [9, 40]. Assuming zero-degree mask angle, our calculation based on precise GLONASS ephemeris data shows that on average it is only a 53% chance for a GLONASS satellite to be in the view of at least one of the monitor stations. As shown by the left plot in Figure 13, the orbit-error-only SIS UREs show a consistent geographic dependency: the UREs when the satellites were monitored are about 0.1-meter less than those when the satellites were unmonitored. However, as shown by the right plot in Figure 13, with clock errors, the SIS UREs no longer show such a consistent geographic dependency: for some satellites like GLONASS-M 731 and 737, the UREs when the satellites were monitored are about 1.5-meter less than those when the satellites were unmonitored; for some satellites like GLONASS-M 719 and 733, the UREs when the satellites were monitored are about 0.4-meter greater than those when the satellites were unmonitored. This paradox may imply some irregular behavior of GLONASS onboard clocks.

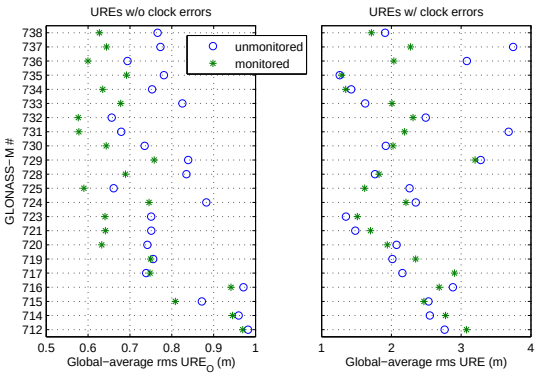

Figure 13. Geographic dependency of GLONASS SIS UREs.

SUMMARY

In this paper, we characterized GLONASS broadcast clock errors and SIS UREs over the past three years with respect to long-term stationarity, mean and standard deviation, distribution, correlation among satellites, and geographic dependency. The statistical characterization is based on the broadcast and precise GLONASS ephemerides and clocks from IGS. One of the contributions of this paper is a clock alignment algorithm to generate correct clock errors from precise clock solutions with unknown time-variant common biases.

For the sake of solid statistics on nominal SIS behavior, this paper considers only the satellites active for at least one year and the healthy SIS that resulted in worst-case UREs less than 50 meters. The statistics show that

- Except a few satellites, the GLONASS SIS URE performance was stationary during the past three years;
- Clock errors dominate SIS URE behavior;
- Mean of clock errors and SIS UREs are nonzero for most satellites, and even exceeds ±1 standard deviation;
- Clock errors and SIS UREs have heavier tails than Gaussian distribution for most satellites;
- UREs of different satellites are usually slightly correlated, but the heavy tail may imply large UREs occasionally occurring on several satellites simultaneously;
- SIS URE performance, especially ephemeris error performance is partially dependent on whether the satellite is monitored.

Although the observed performance of the GLONASS SIS does not quite match the observed performance of GPS [17], the GLONASS SIS are accurate to the 1.5–4 meters level, and the availability of these additional ranging sources will be very beneficial to many multi-constellation GNSS applications.

ACKNOWLEDGMENTS

The authors gratefully acknowledges the support of the Federal Aviation Administration under Cooperative Agreement 08-G-007. This paper contains the personal comments and beliefs of the authors, and does not necessarily represent the opinion of any other person or organization.

REFERENCES

[1] GLONASS constellation status, Accessed February 2012. [Online]. Available: http://www.glonass-ianc.rsa.ru/en/GLONASS/

[2] S. Revnivykh, "GLONASS status and modernization," in *Proceedings of the 24th International Technical Meeting of the Satellite Division of the Institute of Navigation (ION GNSS 2011)*, Portland, OR, September 2011, pp. 839–854.

[3] S. Pullen, G. X. Gao, C. Tedeschi, and J. Warburton, "The impact of uninformed RF interference on GBAS and potential mitigations," in *Proceedings of the 2012 International Technical Meeting of the Institute of Navigation (ION ITM 2012)*, Newport Beach, CA, January 2012.

[4] S. Dosso, M. Vinnins, G. Lachapelle, G. Heard, and E. Cannon, "High latitude attitude," *GPS World*, October 2003.

[5] G. X. Gao, L. Heng, T. Walter, and P. Enge, "Breaking the ice: Navigating in the Arctic," in *Proceedings of the 24th International Technical Meeting of the Satellite Division of the Institute of Navigation (ION GNSS 2011)*, Portland, OR, September 2011, pp. 3767–3772.

[6] S. Hewitson and J. Wang, "GNSS receiver autonomous integrity monitoring (RAIM) performance analysis," *GPS Solutions*, vol. 10, pp. 155–170, 2006.

[7] M. Choi, J. Blanch, D. Akos, L. Heng, G. Gao, T. Walter, and P. Enge, "Demonstrations of multi-constellation Advanced RAIM for vertical guidance using GPS and GLONASS signals," in *Proceedings of the 24th International Technical Meeting of the Satellite Division of the Institute of Navigation (ION GNSS 2011)*, Portland, OR, September 2011, pp. 3227–3234.

[8] P. Misra and P. Enge, *Global Positioning System: Signals, Measurements, and Performance*, 2nd ed. Lincoln, MA: Ganga-Jamuna Press, 2006.

[9] S. Revnivykh, "GLONASS status and progress," in *Proceedings of the 23rd International Technical Meeting of the Satellite Division of the Institute of Navigation (ION GNSS 2010)*, Portland, OR, September 2010, pp. 609–633.

[10] T. Creel, A. J. Dorsey, P. J. Mendicki, J. Little, R. G. Mach, and B. A. Renfro, "Summary of accuracy improvements from the GPS legacy accuracy improvement initiative (L-AII)," in *Proceedings of the 20th International Technical Meeting of the Satellite Division of the Institute of Navigation (ION GNSS 2007)*, Fort Worth, TX, September 2007, pp. 2481–2498.

[11] G. Wübbena, M. Schmitz, G. Boettcher, and C. Schumann, "Absolute GNSS antenna calibration with a robot: Repeatability of phase variations, calibration of GLONASS and determination of carrier-to-noise pattern," in *Proceedings of the IGS Workshop*, 2006.

[12] J. Zumberge and W. Bertiger, "Ephemeris and clock navigation message accuracy," in *Global Positioning System: Theory and Applications*, B. Parkinson, J. Spilker, P. Axelrad, and P. Enge, Eds. Washington, DC: American Institute of Aeronautics and Astronautics, 1996, vol. I, pp. 585–699.

[13] R. B. Langley, H. Jannasch, B. Peeters, and S. Bisnath, "The GPS broadcast orbits: an accuracy analysis," in *33rd COSPAR Scientific Assembly*, Warsaw, Poland, July 2000.

[14] D. M. Warren and J. F. Raquet, "Broadcast vs. precise GPS ephemerides: a historical perspective," *GPS Solutions*, vol. 7, pp. 151–156, 2003.

[15] T. Walter, J. Blanch, and P. Enge, "Evaluation of signal in space error bounds to support aviation integrity," in *Proceedings of the 22nd International Technical Meeting of the Satellite Division of the Institute of Navigation (ION GNSS 2009)*, Savannah, GA, September 2009, pp. 1317–1329.

[16] J. C. Cohenour and F. van Graas, "GPS orbit and clock error distributions," *NAVIGATION*, vol. 58, no. 1, pp. 17–28, Spring 2011.

[17] L. Heng, G. X. Gao, T. Walter, and P. Enge, "Statistical characterization of GPS signal-in-space errors," in *Proceedings of the 2011 International Technical Meeting of the Institute of Navigation (ION ITM 2011)*, San Diego, CA, January 2011, pp. 312–319.

[18] K. Kovach, J. Berg, and V. Lin, "Investigation of upload anomalies affecting IIR satellites in October 2007," in *Proceedings of the 21st International Technical Meeting of the Satellite Division of the Institute of Navigation (ION GNSS 2008)*, Savannah, GA, September 2008, pp. 1679–1687.

[19] J. Lee, "Results on test of URA validation protocol using NGA data," in *GEAS Working Group*, May 2009.

[20] G. X. Gao, H. Tang, J. Blanch, J. Lee, T. Walter, and P. Enge, "Methodology and case studies of signal-in-space error calculation top-down meets bottom-up," in *Proceedings of the 22nd International Technical Meeting of the Satellite Division of the Institute of Navigation (ION GNSS 2009)*, Savannah, GA, September 2009, pp. 2824–2831.

[21] L. Heng, G. X. Gao, T. Walter, and P. Enge, "GPS ephemeris error screening and results for 2006–2009," in *Proceedings of the 2010 International Technical Meeting of the Institute of Navigation (ION ITM 2010)*, San Diego, CA, January 2010, pp. 1014–1022.

[22] ——, "GPS signal-in-space anomalies in the last decade: Data mining of 400,000,000 GPS navigation messages," in *Proceedings of the 23rd International Technical Meeting of the Satellite Division of the Institute of Navigation (ION GNSS 2010)*, Portland, OR, September 2010, pp. 3115–3122.

[23] E. G. Oleynik, V. V. Mitrikas, S. G. Revnivykh, A. I. Serdukov, E. N. Dutov, and V. F. Shiriaev, "High-accurate GLONASS orbit and clock determination for the assessment of system performance," in *Proceedings of the 19th International Technical Meeting of the*

Satellite Division of the Institute of Navigation (ION GNSS 2006), Fort Worth, TX, September 2006, pp. 2065–2079.

[24] R. Píriz, D. Calle, A. Mozo, P. Navarro, D. Rodríguez, and G. Tobías, "Orbits and clocks for GLONASS precise-point-positioning," in *Proceedings of the 22nd International Technical Meeting of the Satellite Division of the Institute of Navigation (ION GNSS 2009)*, Savannah, GA, September 2009, pp. 2415–2424.

[25] H. Yamada, T. Takasu, N. Kubo, and A. Yasuda, "Effect of GLONASS orbit error on long baseline GPS/GLONASS RTK," in *Proceedings of the 22nd International Technical Meeting of the Satellite Division of the Institute of Navigation (ION GNSS 2009)*, Savannah, GA, September 2009, pp. 3290–3296.

[26] L. Heng, G. X. Gao, T. Walter, and P. Enge, "Statistical characterization of GLONASS broadcast ephemeris errors," in *Proceedings of the 24th International Technical Meeting of the Satellite Division of the Institute of Navigation (ION GNSS 2011)*, Portland, OR, September 2011, pp. 3109–3117.

[27] J. M. Dow, R. E. Neilan, and C. Rizos, "The International GNSS Service in a changing landscape of global navigation satellite systems," *Journal of Geodesy*, vol. 83, pp. 689–689, 2009.

[28] IGS formats, Accessed January 2012. [Online]. Available: http://igscb.jpl.nasa.gov/components/formats.html

[29] Russian Institute of Space Device Engineering, *GLONASS Interface Control Document*, 2008.

[30] CDDIS, Accessed January 2012. [Online]. Available: http://igscb.jpl.nasa.gov/components/dcnav/cddis_data_daily_yyg.html

[31] L. Heng, "GLONASS signal-in-space anomalies in the past three years," submitted to the 25th International Technical Meeting of the Satellite Division of the Institute of Navigation (ION GNSS 2012).

[32] IGS Products, Accessed January 2012. [Online]. Available: http://igscb.jpl.nasa.gov/components/prods.html

[33] P. W. Holland and R. E. Welsch, "Robust regression using iteratively reweighted least-squares," *Communications in Statistics: Theory and Methods*, vol. 6, no. 9, pp. 813–827, 1977.

[34] A. M. Gross, "Confidence intervals for bisquare regression estimates," *Journal of the American Statistical Association*, vol. 72, no. 358, pp. 341–354, June 1977.

[35] L. Heng, G. X. Gao, T. Walter, and P. Enge, "GPS signal-in-space integrity performance evolution in the last decade: Data mining 400,000,000 navigation messages from a global network of 400 receivers," *IEEE Transactions on Aerospace and Electronic Systems*, accepted for publication.

[36] US DoD, *Global Positioning System Standard Positioning Service Performance Standard*, 3rd ed., October 2001.

[37] H. C. Thode, *Testing for Normality*. New York, NY: Marcel Dekker, 2002.

[38] J. W. Pratt, H. Raiffa, and R. Schlaifer, *Introduction to Statistical Decision Theory*. The MIT Press, 1995.

[39] J. Rife, S. Pullen, B. Pervan, and P. Enge, "Paired overbounding and application to GPS augmentation," in *Proceedings of 2004 IEEE/ION Position Location and Navigation Symposium (PLANS 2004)*, Monterey, CA, April 2004, pp. 439–446.

[40] R. B. Langley, "GLONASS update delves into constellation details," *GPS World*, September 2010. [Online]. Available: http://www.gpsworld.com/gnss-system/glonass/news/glonass-update-delves-constellation-details-10499